IEEE Photonics Journal
An IEEE Photonics Society Publication

Highly Polarized Fluorescent Film Based on Aligned Quantum Rods by Contact Ink-Jet Printing Method

Volume 11, Number 2, April 2019

Ziming Zhou
Kai Wang, *Member, IEEE*
Zhe Zhang
Chaojian Zhang
Haochen Liu
Yang Zhang
Zuoliang Wen
Shang Li
Junjie Hao
Bing Xu
Stephen John Pennycook
Kie Leong Teo, *Member, IEEE*
Xiao Wei Sun, *Senior Member, IEEE*

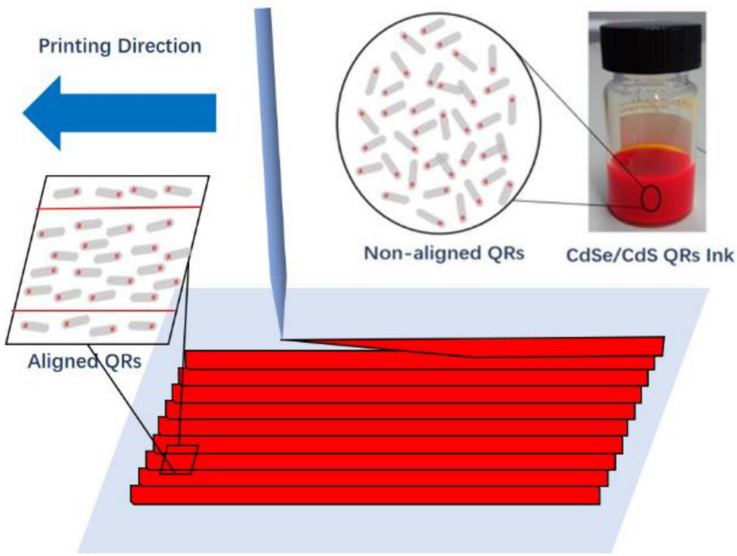

DOI: 10.1109/JPHOT.2019.2902313
1943-0655 © 2019 IEEE

IEEE photonics SOCIETY
IEEE

Highly Polarized Fluorescent Film Based on Aligned Quantum Rods by Contact Ink-Jet Printing Method

Ziming Zhou,[1,2] Kai Wang,[1] *Member, IEEE*, Zhe Zhang,[1] Chaojian Zhang,[1] Haochen Liu,[1] Yang Zhang,[3] Zuoliang Wen,[1,2] Shang Li,[1,4] Junjie Hao,[1,4] Bing Xu,[1,4] Stephen John Pennycook,[3] Kie Leong Teo,[2] *Member, IEEE*, and Xiao Wei Sun,[1] *Senior Member, IEEE*

[1]Guangdong University Key Lab for Advanced Quantum Dot Displays and Lighting, Shenzhen Key Laboratory for Advanced Quantum Dot Displays and Lighting, Department of Electrical & Electronic Engineering, Southern University of Science and Technology, Shenzhen 518055, China
[2]Department of Electrical and Computer Engineering, National University of Singapore, Singapore 117583
[3]Department of Materials Science and Engineering, National University of Singapore, Singapore 117575
[4]Shenzhen Planck Innovation Technologies, Shenzhen 518112, China

DOI:10.1109/JPHOT.2019.2902313

Manuscript received January 31, 2019; accepted February 24, 2019. Date of publication February 28, 2019; date of current version March 14, 2019. This work was supported in part by the National Key Research and Development Program of China administrated by the Ministry of Science and Technology of China under Grant 2016YFB0401702, in part by the National Natural Science Foundation of China under Grant 61674074 and Grant 61405089l, in part by the Distinguished Young Scholar of Natural Science Foundation of Guangdong (No. 2017B030306010), in part by the Shenzhen Peacock Team Project under Grant KQTD2016030111203005, in part by the Shenzhen Innovation Project under Grant JCYJ20160301113356947 and Grant JCYJ20160301113537474, in part by the Doctoral Fund of Ministry of Education of China (No. 2017M610484 and 2017M612497), in part by the Shenzhen Key Lab of Advanced Quantum Dot Displays and Lighting, in part by the Guangdong Higher Education Key Lab of Advanced Quantum Dot Displays and Lighting, and in part by the Development and Reform Commission of Shenzhen Municipality. This work was also supported by the Pico Center at SUSTech that receives support from Presidential fund and Development and Reform Commission of Shenzhen Municipality. Corresponding authors: Kai Wang, Kie Leong Teo and Xiao Wei Sun (e-mail: wangk@sustc.edu.cn; eleteokl@nus.edu.sg; sunxw@sustc.edu.cn).

Abstract: Fluorescent quantum rods (QRs) have received much attention recently because of their properties of polarized light emission with narrow full width at half-maximum. Therefore, QRs can be used in liquid crystal display (LCD) backlight, as an active polarizer. In order to emit light with a high degree of polarization (DOP), QRs need to be controlled and aligned along one direction on large-scaled devices. However, most of the proposed effective alignment approaches cannot be applied to a large area. In this paper, we report for the first time the contact ink-jet printing (CIJP) method to align CdSe/CdS core/shell QRs. With the ink being printed, the QRs can align along the fluid ink flow direction resulting in aligned QRs along printing direction and forming a film with a high DOP of 42%. Furthermore, CIJP can realize arbitrarily large area fabrication without reducing DOP value. It is expected that this method can be utilized to print on large-scaled substrates directly to fabricate polarized optoelectronic devices, and further applied to LCD backlights and any other applications where polarized light is needed.

Index Terms: Alignment, contact ink-jet printing, polarization, quantum rods.

1. Introduction

Fluorescent semiconductor quantum rods (QRs) are brought into focus and applied in many photoelectric devices including liquid crystal (LC) display backlights [1], [2]–[4], LC cells [4]–[6], light emitting diodes (LEDs) [7]–[9], microcavities and lasers [10]–[14], solar cells [15]–[17], luminescent solar concentrators (LSC) [18]–[20], and other applications including photocatalytic hydrogen generation [21]–[23] and bioimaging [24]–[27]. Because there are a lot of outstanding properties of QRs covering tunable emission, polarized emission, narrow full width at half maximum (FWHM), and large quasi-Stokes shift [20], [28], [29]. And the improved core/shell QRs not only retain these properties and high polarization, but also exhibit high quantum efficiency [30]–[32].

Compared with traditional semiconductor quantum dots, the most useful but most difficult to be utilized property of QRs is the polarized emission. The degree of polarization (DOP) of emission is defined by $(I_{\parallel} - I_{\perp})/(I_{\parallel} + I_{\perp})$, where $I_{\parallel}$ and $I_{\perp}$ are the photo-luminescent (PL) intensities of the polarized light parallel and perpendicular to the long axis of the quantum rod, respectively [33]. As the aspect ratio (AR) of single quantum rod increases from 1:1 to 10:1, the DOP of emission increases from $<$0.1 up to 0.86 [29]. However, colloidal QRs are generally random in orientation, hence different quantum rods will emit random polarized light so that the DOP of colloidal QRs is very small. Therefore, the polarized emission property of QRs can be utilized in practice, only if the QRs can be aligned perfectly and emit light with a high DOP.

For these reasons, a lot of researchers are working on the alignment of QRs through different methods to achieve high DOP in large-scale. The alignment strategies include photo-illumination [34]–[36], applying electrical field [37]–[40], evaporation [41], [42], Langmuir-Blodgett (LB) assembly [43], [44], coffee stain effect [12], [13], [45], capillary effect [11], superlattice [46], [47], nanostructure assisted assembly [48]–[50], electrospinning [1], [3], [51], rubbing [9], [52], [53], stretching [2], [9], and vertical growth [16], [54]. However, all of these methods are not perfect enough. The growth and evaporation methods can align QRs vertically, which cannot be applied as a planar device. Although LB assembly method can align QRs horizontally, the achieved maximal DOP of emitted light from aligned film is 0.34 [8]. Although coffee stain effect, capillary effect, superlattice methods can aligned QRs perfectly within some small regions, the achieved maximal width of aligned QRs is less than 150 μm, which cannot be utilized into devices [11]. Although QR alignments by photo-illumination, electrical field, nanostructure-assisting, electro-spinning, stretching and rubbing etc. can achieve high DOP with large areas, these methods have not tested for different substrates (e.g., plastics) with different form factors (e.g., curved). Thus it is always worthwhile to develop new QR alignment techniques. In this work, we firstly put forward by using the contact ink-jet printing (CIJP) method to align CdSe/CdS QRs. Actually, this method is similar to the capillary printing method, which has been used to align nanowires. [55], [56] Thanks to the natural advantages of CIJP, this method can print QRs on different materials and shapes of substrates in arbitrarily large area, and achieve DOP of emitted light with DOP higher than 0.42. This new method could be utilized to realize useful devices with highly polarized light emission.

2. Experimental Section

In this study, a CdSe dot in a CdS rod-shaped shell was grown based on the method reported with some modifications [37]. Through the two-sequential seed-grown process, the emission and aspect ratio of dot-in-rod QRs can be controlled well, and high quantum yield and narrow FWHM can be achieved at the same time.

2.1 Chemicals

Selenium powder (Se, 99.999%, 100 mesh) was purchased from Alfa Aesar. Cadmium oxide (CdO, 99.99%) and sulfur powder (S, 99.999%) were purchased from Aladdin. Trioctylphosphine (TOP, 97%), tetradecylphosphonic acid (TDPA, 97%), trioctylphosphine oxide (TOPO, 99%), and n-hexylphosphonic acid (HPA, 97%) were purchased from Strem Chemicals. 1, 2-dichlorobenzene

(o-DCB, 99%) was purchased from Sigma Aldrich. All the chemicals were used as received without further purification.

2.2 Preparation of Se- and S-Precursors

Se- and S- precursors were both prepared in the glove box with argon atmosphere. 1.184 g of Se powder and 15 ml of TOP were mixed in an uncontaminated vial. Afterwards, the mixture was stirred by a magnetic stir bar at room temperature for more than 8 h, until the Se powder was completely dissolved into TOP to become the 1 mmol/ml Se-TOP solution. 1.202 g of S powder and 15 ml of TOP were mixed in another uncontaminated vial. And then, the mixture was stirred by a magnetic stir bar with 110 °C heating for more than 8 h, until the S powder was absolutely dissolved into TOP to form the 2.5 mmol/ml S-TOP solution. At last, these prepared precursors were reserved in glove box at room temperature.

2.3 Synthesis and Purification of CdSe Cores

Firstly, 90 mg of CdO, 0.420 g of TDPA and 4.5 g of TOPO were orderly put into a 50 ml three-necked flask followed with 150 °C heating. When the temperature reached 75 °C, the mixture started to be stirred by a high temperature magnetic stir bar with the speed of 400 rpm. Then, the temperature of the whole system arrived and maintained at 150 °C, after which, the atmosphere in flask was alternately changed between vacuum and argon for more than 6 times, until no bubbles emerged from the mixture and all the chemicals became liquid except CdO. After the atmosphere exchange, argon was full of the whole flask. Next, the mixture was further heated to 320 °C, at which point CdO dissolved into solution and make the liquid transparent. When the solution was totally colorless, 0.25 ml of TOP was injected into the flask. Then, the solution was heated to 370 °C gradually, and 1 ml of Se-TOP was rapidly injected into the flask just when 370 °C was reached. After 20 s, the flask was immediately removed from heating mantle and was naturally cooled down to 70∼80 °C. Finally, these prepared CdSe cores were washed and purified by the mixture of ethanol and chloroform (or toluene) as well as centrifugation (10000 rpm, 3 min) for at least two times, and the eventual precipitate was dispersed into TOP to become CdSe-TOP.

2.4 Synthesis and Purification of CdSe/CdS Core/Shell QRs

At first, 115.8 mg of cadmium oxide, 162 mg of HPA, 600 mg of TDPA and 6 g of TOPO were sequentially put into a 100 ml three-necked flask followed with 150 °C heating. When the temperature reached 75 °C, the mixture started to be stirred by a high temperature magnetic stir bar with the speed of 400 rpm. Then, the same atmosphere exchange process described previously was carried out at 150 °C. Next, the mixture was further heated to 300 °C, at which point CdO dissolved into solution and make the liquid completely colorless, followed by the injection of 3 ml TOP. Afterwards, the solution was heated to 320 °C gradually, and the mixture of 3 ml TOP and 112 nmol CdSe dispersed in TOP was speedily injected into the flask just when 320 °C was reached. After 8 min, the flask was immediately removed from heating mantle and was naturally cooled down to 70∼80 °C. At last, these prepared CdSe/CdS dot-in-rod QRs were washed and purified by the mixture of ethanol and chloroform as well as centrifugation (10000 rpm, 3 min) for at least two times, and the eventual precipitate was dispersed into toluene with the concentration of 3 mg/ml.

2.5 Preparation of QRs Ink

First of all, 3 ml of o-DCB was added into 8 ml CdSe/CdS QRs toluene solution, and some of the QRs were separated out caused by their small solubility in o-DCB. Afterwards, the mixture was heated in a 60 °C thermostatic oven for 30 min, and then, stood at room temperature until the supernatant was lucid. Finally, the supernatant was extracted carefully by pipettes to an uncontaminated vial as the QRs ink.

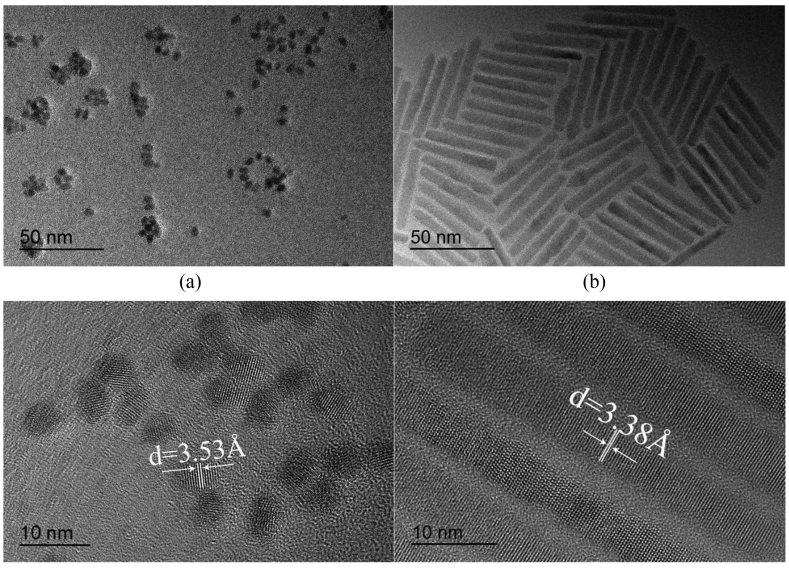

Fig. 1. Low resolution TEM images of (a) CdSe cores and (b) CdSe/CdS QRs. HRTEM images of (c) CdSe cores with a lattice constant of 3.53 Å and (d) CdSe/CdS QRs with a lattice constant of 3.38 Å.

2.6 Fabrication of QRs Film by CIJP

The QRs film was fabricated by an ink-jet printing machine (GIX Microplotter II, SonoPlot). At the beginning, 100 μl of the prepared QRs ink was stored in an uncontaminated container. The 10 μm pinhead was used to firstly calibrate the slope of the substrate in order to make the printing more smoothly. Next, the capillary tip was adjusted to the start point, where the tip exactly contacted with substrate, with the help of a microscope. After recorded the coordinate of the start point, the pit was moved to the position of ink container, and the QRs ink would be automatically sucked into pinhead caused by the capillary force. Afterwards, the capillary was immediately manipulated to the start point and began printing with the speed of 500 μm/s. Eventually, the machine printed the whole QRs film on the substrate followed the setup printing pattern automatically.

3. Results and Discussions

The size, shape and crystalline structure of the synthesized CdSe/CdS core/shell QRs are characterized by transmission electron microscope (TEM, FEI Tecnai G2 F30), high resolution TEM (HRTEM, FEI Tecnai G2 F30) and X-Ray Diffraction (XRD, Bruker Advance D8 Ew, Germany). As shown in Fig. 1(a) and 1(b), both CdSe quantum dots (QDs) and CdSe/CdS QRs were monodispersed and had uniform size. The more detailed information was demonstrated by HRTEM images of QDs and QRs, which are shown in Fig. 1(c) and 1(d), respectively. Compared with CdSe cores, the CdSe/CdS QRs obviously became wider and elongated, which confirms the formation of CdS shells. The diameters of QDs are 4.2 $\pm$ 0.3 nm, and the diameters and the lengths of QRs are 5.8 $\pm$ 0.5 nm and 49 $\pm$ 2.5 nm, respectively, with the aspect ratio of around 8:1. Through fast Fourier transform (FFT) analysis of the HRTEM images, the d-spacing of the adjacent crystal planes perpendicular to the c-axis of CdSe core and CdSe/CdS rod are 3.53 Å and 3.38 Å, respectively. CdSe core has bigger lattice constant because of the larger size of Se atom. As shown in Fig. 2, CdSe cores and CdSe/CdS QRs were also characterized by XRD analysis, and the XRD spectra and corresponding diffraction peaks of cores and QRs are matched well with wurtzite CdSe (JCPDF No. 02-0330) and wurtzite CdS (JCPDF No. 41-1049), respectively. The results demonstrate that, as the shells were grown on the cores, not only the crystalline structures detected were changed from pure CdSe wurtzite crystals to pure CdS wurtzite crystals, but also the diffraction peaks, such

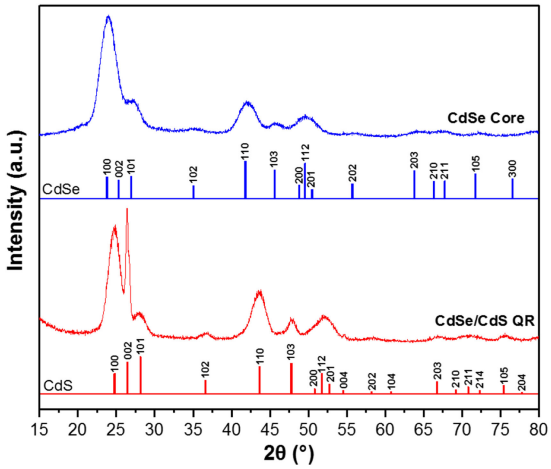

Fig. 2. X-ray diffraction (XRD) results of powdered samples of CdSe cores (upper line) and CdSe/CdS QRs (lower line). The XRD PDF standard card of CdSe (upper bars, JCPDF of No. 02-0330) and CdS (lower bars, JCPDF of No. 41-1049) are also exhibited under XRD results, respectively, as the references.

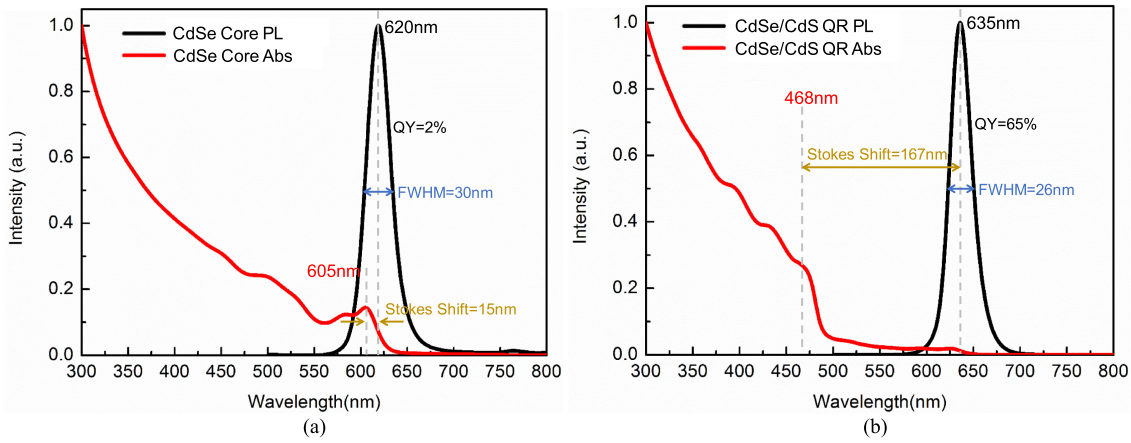

Fig. 3. UV-vis absorption and PL spectra excited by 450 nm monochromatic light of (a) CdSe cores with a Stokes shift of 15nm and (b) CdSe/CdS QRs with a quasi-Stokes shift of 167 nm.

as (100), (101) and (110), have a slight shift towards larger 2θ direction due to the less lattice plane spacings of CdS shells. Calculated from the XRD spectra, the d-spacing of the adjacent crystal planes perpendicular to the c-axis of CdSe core and CdSe/CdS rod are 3.50 Å and 3.37 Å, respectively, which are in accordance with the values obtained from HRTEM images. Integrating both TEM images and XRD spectra, the structure and morphology of a wurtzite CdSe core in a wurtzite CdS rod-like shell can be clearly envisioned.

The optical properties of CdSe cores and CdSe/CdS QRs were characterized by the room temperature ultraviolet-visible (UV-Vis) spectrophotometer (PerkinElmer Lambda950) and PL spectroscopy (Hamamatsu Quantaurus-QY C11347-12). As shown in Fig. 3(a), we can see that the first exciton absorption peak is at 605 nm, and the emission at 620 nm has an FWHM of 30 nm. With the CdSe cores being coated by CdS shells, as shown in Fig. 3(b), the PL quantum yield (QY) increases from 2% to 65%, because the CdS shell structures repair most of the defects on the surface of CdSe cores. At the same time, the absorption peak has a blue-shift of 137 nm; the emission peak has a red-shift of 15 nm; and the FWHM of emission has shrinked 4 nm. As a result, QRs will have less self-absorption effects compared to its core or core/shell QD counterparts [20].

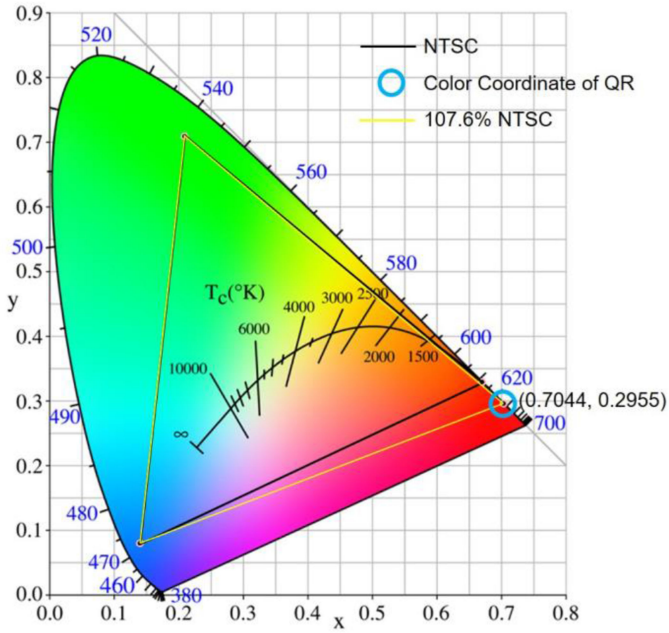

Fig. 4. The CIE 1931 color coordinates of standard NTSC (black line) and CdSe/CdS QRs synthesized through TBP-assisted method (yellow line).

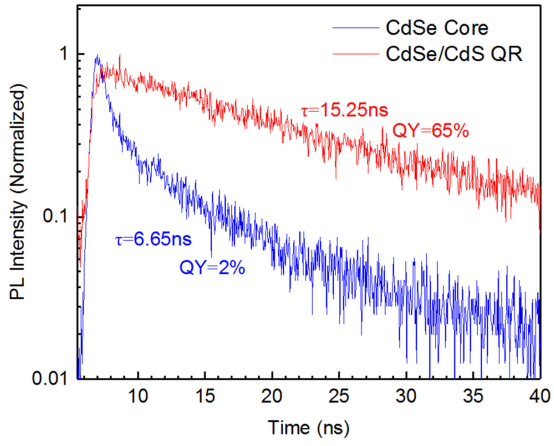

Fig. 5. Time-resolved photo-luminescent decay of CdSe cores and CdSe/CdS QRs. The corresponding absolute QY and lifetime are inserted beside data with a same color.

As shown in Fig. 4, the commission internationale de l'eclairage (CIE) color coordinates of these QRs, (0.7063, 0.2934), was calculated from the emission spectra of QRs. If this kind of QRs can be used to substitute the standard red color coordinates, (0.67, 0.33), of national television standards committee (NTSC), the color gamut will become up to 107.6% of NTSC. Therefore, the LCD devices incorporating this kind of aligned QRs film could have a wider color gamut.

The properties of exciton recombination in QRs were also characterized by time-resolved PL spectroscopy (Edinburgh Instruments FLS-980), which is shown in Fig. 5. From the PL lifetime measurement, it is seen that the spectra of CdSe/CdS core/shell QRs can be fitted by a single exponential function, and the PL lifetime of the QRs was calculated as 12.25 ns with a goodness-of-fit (χ^2) of 0.989. This means that there is approximately only one channel for the excited states relaxation, which is radiative recombination. This is one of the reasons for a high quantum yield.

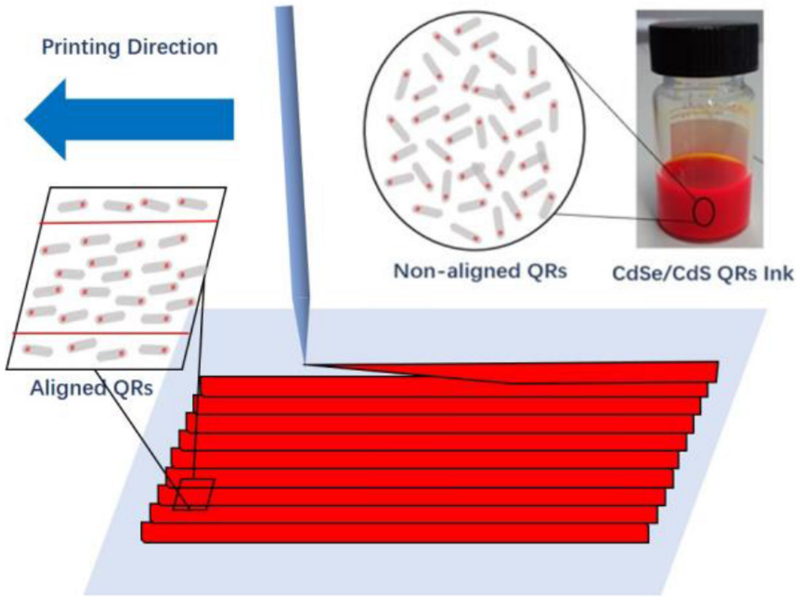

Fig. 6. Schematic diagram of CIJP alignment method.

Another reason for the high yield is the CdSe/CdS has a quasi-Type II band structure, leading to a less overlap between the electron and hole wavefunctions. [30], [57] In contrast, the spectra of core-only CdSe QDs can only be well fitted by two exponential functions, and the two lifetimes associated were calculated as 0.8625 ns (weighting factor of 21.61%) and 8.2398 ns (weighting factor of 78.39%) with a χ^2 of 1.143. Therefore, the total lifetime of CdSe cores was calculated as 6.65 ns. According to the fitting results, it is obvious that CdSe cores have radiative and nonradiative recombination channels. As a result, the CdSe core-only QDs will have a lower quantum yield. It is worth mentioning that the core-only QDs have different band structures from the core/shell counterparts, it should be considered as a Type-I structure (with solvent/ligands as its shell). As a result, the core-only QDs have a shorter lifetime, and a lower quantum yield.

Contact ink-jet printing method was adopted to align the synthesized CdSe/CdS QRs to form a film on a glass substrate. The solvent of QRs ink was a mixture of 1, 2-dichlorobenzene (o-DCB) and toluene with optimized volume ratio of 3:8, which do not have any adverse effect on the QY of QRs. Actually, the QY of the QRs ink can reach 62%. Toluene is helpful to increase the concentration of QRs, because QRs have larger solubility in it. On the other hand, o-DCB has a slower volatility benefiting a high quality of film.

The schematic diagram of CIJP alignment method was shown in Fig. 6. Different from conventional ink-jet printing method, CIJP method makes continuous ink jet flow instead of discontinuous drops on substrates, which can induce the QRs float. Initially, the QRs in vial was non-aligned. Once the QRs ink was jetted from the tip while the writing head moved towards left direction, the QRs in the ink will float towards the printing direction driven by the ink flowing. During the process, the QRs tended to align along the printing direction, which is called flow assembly. [58] Eventually, QRs can be aligned almost in the same direction in each printed strip. The printed samples illuminated by white light and UV light was exhibited in Fig. 7(a) and 7(b), respectively. The dimension of print area was 6 mm $\times$ 8 mm, which actually can be extended easily by changing printing program. Moreover, the thickness of the aligned QRs film measured by a stylus profiler (Bruker Dektak XT) was 65 $\pm$ 5 nm. Therefore, as shown in Fig. 7(a), the QRs film are almost transparent under room light, which is more useful where transparency is needed.

The polarization property of this printed QRs film was measured. As shown in Fig. 8(a), a beam of 450 nm monochromatic light is firstly selected from a Xenon lamp by a monochromator,

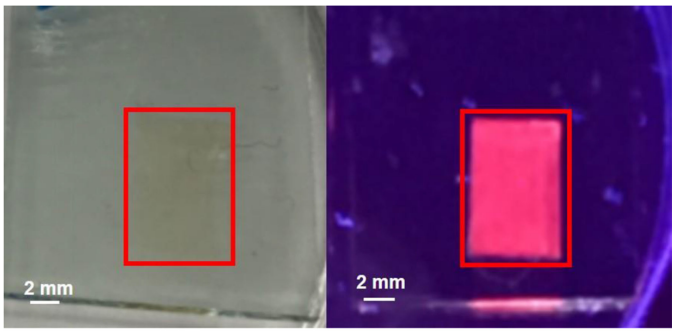

Fig. 7. Exhibition of the QRs film sample fabricated by CIJP method without under (a) white light and (b) UV light. (The red frames are print areas.)

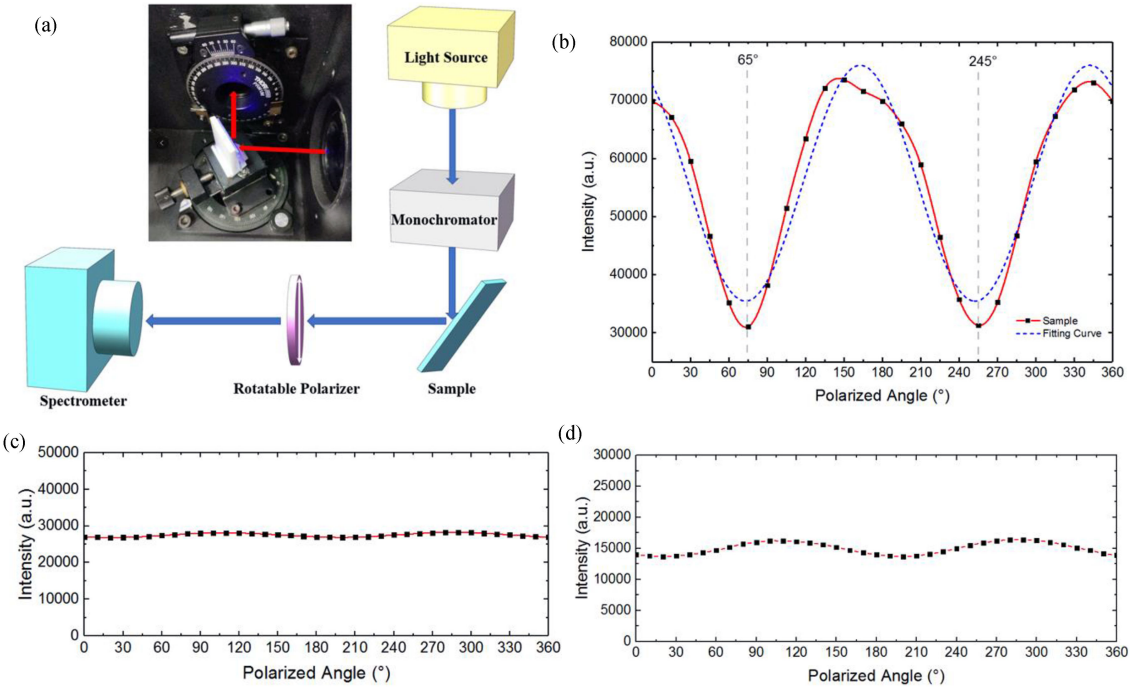

Fig. 8. (a) Photo and schematic diagram of the setup of polarization measurement. Emitted light intensity from (b) contact ink-jet printed QRs film (anisotropic), (c) spin-coated QDs film (isotropic) and (d) spin-coated QRs film (isotropic) as a function of the polarizer angle (solid line). The dot line in (b) is a fitting curve for the polarization result of the aligned QRs film.

and then illuminates on the sample. The sample will absorb the excitation light and emits light in all directions. Part of the emitted light emits towards a rotatable polarizer, and only the linearly polarized light with the same polarization direction of the polarizer can pass through and be detected by the spectrometer. The spectrometer was set only to measure the light from 500 nm to 800 nm to avoid detecting pump beam. By rotating the polarizer, we can determine the DOP of the samples. Firstly, the relationship between emission peak intensity of aligned QRs film and angle of polarizer was exhibited in Fig. 8(b). From the solid line in Fig. 8(c), the DOP value of the fabricated QRs film calculated is 0.42. The achieved high DOP value of this QRs film indicates the CIJP alignment method has much potential to be applied to LCD backlight or even many other optoelectronic devices. And the experimental data can be fitted by a $\cos^2$ function (dash line) very well. According

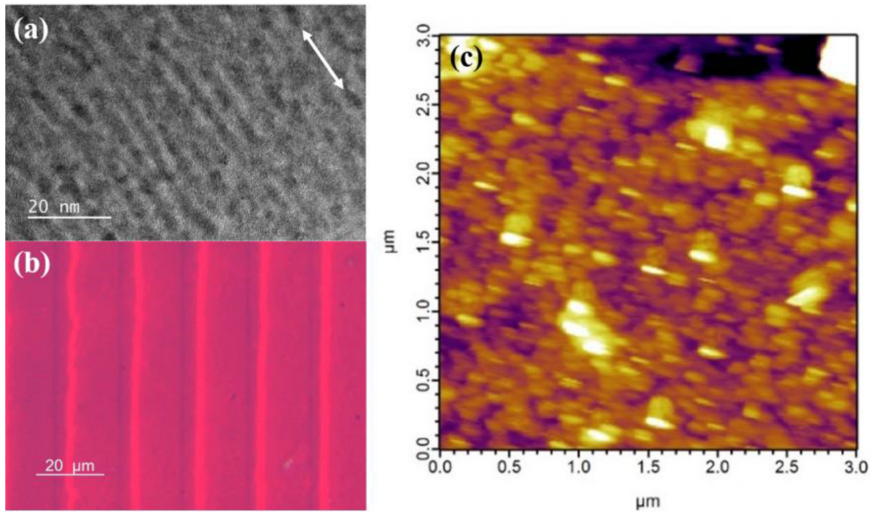

Fig. 9. (a) TEM image of the aligned CdSe/CdS core/shell QR sample by CIJP method. The arrow in the image presents printing direction. (b) Fluorescence microscope image and (c) AFM image of the aligned QRs film.

to the Malus Law, this implicates the partially polarized light emission from the film and the effective alignment of QRs. [59] As shown in Fig. 8(c), we used this setup to measure a CdSe/ZnS Quantum dots film, which is almost isotropic, fabricated by spin-coating, and obtained the DOP of this film is only 2.52%. This result can demonstrate that there is almost no effect caused by the response anisotropy of the monochromator in this setup. For comparison purpose, we also measured the DOP of a spin-coated CdSe/CdS QR film as shown in Fig. 8(d). It can be seen that the DOP of this film is 8.25%, which is much smaller than that of CIJP aligned QR film as expected. It is worth mentioning that the DOP value of spin-coated QR film (8.25%) is larger than that of QD film (2.52%). This is probably because the measured area of the sample can hardly overlap with the spinning center during spin-coating. There remains some alignment of QRs along the radial direction of the circular spinning.

The alignment of the CdSe/CdS core/shell QRs was also characterized directly by TEM. The plan-view TEM sample was prepared with the following steps: (1) cover a thin epoxy layer with a larger area on the film to fix the film onto the substrate, since the contact between the film and the substrate is weak; (2) grind and polish the epoxy layer side close to the film; (3) grind and polish the substrate; (4) ion mill the substrate side using Fischione M1051. The TEM observation was performed on JEOL ARM200F in National University of Singapore. As shown in Fig. 9(a), although the TEM image is not very clear, because the aligned QRs film on glass substrate are not monolayered, nevertheless, it is also obvious that the QRs are aligned very well along the direction of printing marked in Fig. 9(a). Furthermore, the fluorescence microscope image of the aligned QRs film was shown in Fig. 9(b). The printed lines contact with each other, and in fact the neighboring lines share a small overlap. If the lines are in contact to each other, the rods will still align on the printing direction, because printing QRs in the continuous ink jet fluid is just like flowing logs in a river. We have also measured the atomic force microscope (AFM) image of the aligned QRs film as shown in the following Fig. 9(c). The root-mean-square roughness calculated from the AFM picture is 6.247nm. From the figure, we can see vaguely some aligned structures of rod-like shape.

4. Conclusions

In summary, we report a contact ink-jet printing method to align CdSe/CdS core/shell QRs for the first time. The synthesized QRs with emission of 635 nm, FWHM of 26 nm, and absolute QY of

65% were dispersed in the mixture of toluene and o-DCB as the ink. Then, as the QRs ink was printed by CIJP method, the QRs flew and aligned along the axes of print paths. The obtained QRs film has a high DOP of 0.42. Compared other alignment methods, CIJP alignment are naturally more flexible. It not only can fabricate almost transparent QRs film in large area even industrial manufacture, but also can achieve printing on any substrate with any form factor, just like the 3D printing. It is expected that this method has great potential to be applied to LCD backlight and other optical or optoelectronic devices.

References

[1] M. Hasegawa and Y. Hirayama, "Use of quantum rods for display applications," *J. Soc. Inf. Display*, vol. 24, no. 5, pp. 286–292, May 2016.
[2] P. D. Cunningham, J. B. Souza, I. Fedin, C. X. She, B. Lee, and D. V. Talapin, "Assessment of anisotropic semiconductor nanorod and nanoplatelet heterostructures with polarized emission for liquid crystal display technology," *ACS Nano*, vol. 10, no. 6, pp. 5769–5781, Jun. 2016.
[3] T. Aubert *et al.*, "Large-scale and electroswitchable polarized emission from semiconductor nanorods aligned in polymeric nanofibers," *ACS Photon.*, vol. 2, no. 5, pp. 583–588, May 2015.
[4] M. Mohammadimasoudi, J. Beeckman, Z. Hens, and K. Neyts, "Hybrid fluorescent layer emitting polarized light," *APL Mater.*, vol. 5, no. 7, Jul. 2017, Art. No. 076104.
[5] M. Mohammadimasoudi, Z. Hens, and K. Neyts, "Full alignment of dispersed colloidal nanorods by alternating electric fields," *RSC Advances*, vol. 6, no. 61, pp. 55736–55744, 2016.
[6] H. S. Chen *et al.*, "Color-tunable light-emitting device based on the mixture of CDSE nanorods and dots embedded in liquid-crystal cells," *J. Phys. Chem. C*, vol. 114, no. 17, pp. 7995–7998, May 2010.
[7] T. Wang, X. R. Wang, D. LaMontagne, Z. W. Wang, and Y. C. Cao, "Macroscale lateral alignment of semiconductor nanorods into freestanding thin films," *J. Amer. Chem. Soc.*, vol. 135, no. 16, pp. 6022–6025, Apr. 2013.
[8] A. Rizzo *et al.*, "Polarized light emitting diode by long-range nanorod self-assembling on a water surface," *ACS Nano*, vol. 3, no. 6, pp. 1506–1512, Jun. 2009.
[9] R. A. M. Hikmet, P. T. K. Chin, D. V. Talapin, and H. Weller, "Polarized-light-emitting quantum-rod diodes," *Adv. Mater.*, vol. 17, no. 11, pp. 1436–1439, Jun. 2005.
[10] P. Liu *et al.*, "Assembling ordered nanorod superstructures and their application as microcavity lasers," *Sci. Rep.*, vol. 7, Mar. 8, 2017, Art. no. 43884.
[11] Y. Gao *et al.*, "Observation of polarized gain from aligned colloidal nanorods," *Nanoscale*, vol. 7, no. 15, pp. 6481–6486, 2015.
[12] M. Zavelani-Rossi *et al.*, "Self-assembled CdSe/CdS nanorod micro-lasers fabricated from solution by capillary jet deposition," *Laser Photon. Rev.*, vol. 6, no. 5, pp. 678–683, Sep. 2012.
[13] M. Zavelani-Rossi, M. G. Lupo, R. Krahne, L. Manna, and G. Lanzani, "Lasing in self-assembled microcavities of CdSe/CdS core/shell colloidal quantum rods," *Nanoscale*, vol. 2, no. 6, pp. 931–935, 2010.
[14] B. Moller, U. Woggon, M. V. Artemyev, and R. Wannemacher, "Mode control by nanoengineering light emitters in spherical microcavities," *Appl. Phys. Lett.*, vol. 83, no. 13, pp. 2686–2688, Sep. 2003.
[15] F. Qiao *et al.*, "Effect of Cd-phosphonate complex on the self-assembly structure of colloidal nanorods," *Mater. Lett.*, vol. 180, pp. 85–88, Oct. 2016.
[16] M. Wang, J. Jiang, J. Shi, and L. Guo, "CdS/CdSe core-shell nanorod arrays: Energy level alignment and enhanced photoelectrochemical performance," *ACS Appl. Mater. Interfaces*, vol. 5, no. 10, pp. 4021–4025, May 22, 2013.
[17] L. Bian *et al.*, "Hole-induced large-area homoepitaxial growth of CdSe nanowire arrays for photovoltaic application," *J. Mater. Chem. A*, vol. 1, no. 21, pp. 6313–6319, 2013.
[18] D. Sahin, B. Ilan, and D. F. Kelley, "Monte-Carlo simulations of light propagation in luminescent solar concentrators based on semiconductor nanoparticles," *J. Appl. Phys.*, vol. 110, no. 3, Aug. 1, 2011, Art. no. 033108.
[19] L. R. Bradshaw, K. E. Knowles, S. McDowall, and D. R. Gamelin, "Nanocrystals for luminescent solar concentrators," *Nano Lett.*, vol. 15, no. 2, pp. 1315–1323, Feb. 2015.
[20] N. D. Bronstein *et al.*, "Luminescent solar concentration with semiconductor nanorods and transfer-printed micro-silicon solar cells," *ACS Nano*, vol. 8, no. 1, pp. 44–53, Jan. 2014.
[21] F. Qiu, Z. J. Han, J. J. Peterson, M. Y. Odoi, K. L. Sowers, and T. D. Krauss, "Photocatalytic hydrogen generation by CdSe/CdS nanoparticles," *Nano Lett.*, vol. 16, no. 9, pp. 5347–5352, Sep. 2016.
[22] H. J. Lv, T. P. A. Ruberu, V. E. Fleischauer, W. W. Brennessel, M. L. Neidig, and R. Eisenberg, "Catalytic light-driven generation of hydrogen from water by iron dithiolene complexes," *J. Amer. Chem. Soc.*, vol. 138, no. 36, pp. 11654–11663, Sep. 2016.
[23] P. Kalisman, Y. Nakibli, and L. Amirav, "Photochemical oxidative growth of iridium oxide nanoparticles on CdSe@CdS nanorods," *Jove-J. Visualized Experiments*, vol. 108, Feb. 2016, Art. no. e53675.
[24] S. Deka *et al.*, "CdSe/CdS/ZnS double shell nanorods with high photoluminescence efficiency and their exploitation as biolabeling probes," *J. Amer. Chem. Soc.*, vol. 131, no. 8, pp. 2948–2958, Mar. 2009.
[25] K. T. Yong *et al.*, "Multiplex imaging of pancreatic cancer cells by using functionalized quantum rods," *Adv. Mater.*, vol. 20, no. 8, pp. 1412–1417, Apr. 2008.
[26] K. T. Yong *et al.*, "Quantum rod bioconjugates as targeted probes for confocal and two-photon fluorescence imaging of cancer cells," *Nano Lett.*, vol. 7, no. 3, pp. 761–765, Mar. 2007.
[27] A. H. Fu *et al.*, "Semiconductor quantum rods as single molecule fluorescent biological labels," *Nano Lett.*, vol. 7, no. 1, pp. 179–182, Jan. 2007.

[28] A. Sitt, I. Hadar, and U. Banin, "Band-gap engineering, optoelectronic properties and applications of colloidal heterostructured semiconductor nanorods," *Nano Today*, vol. 8, no. 5, pp. 494–513, Oct. 2013.
[29] J. T. Hu, L. S. Li, W. D. Yang, L. Manna, L. W. Wang, and A. P. Alivisatos, "Linearly polarized emission from colloidal semiconductor quantum rods," *Science*, vol. 292, no. 5524, pp. 2060–2063, Jun. 15, 2001.
[30] D. V. Talapin, J. H. Nelson, E. V. Shevchenko, S. Aloni, B. Sadtler, and A. P. Alivisatos, "Seeded growth of highly luminescent CdSe/CdS nanoheterostructures with rod and tetrapod morphologies," *Nano Lett.*, vol. 7, no. 10, pp. 2951–2959, Oct. 2007.
[31] Z. A. Peng and X. G. Peng, "Mechanisms of the shape evolution of CdSe nanocrystals," *J. Amer. Chem. Soc.*, vol. 123, no. 7, pp. 1389–1395, Feb. 2001.
[32] A. Sitt, A. Salant, G. Menagen, and U. Banin, "Highly emissive nano rod-in-rod heterostructures with strong linear polarization," *Nano Lett.*, vol. 11, no. 5, pp. 2054–2060, May 2011.
[33] J. F. Wang, M. S. Gudiksen, X. F. Duan, Y. Cui, and C. M. Lieber, "Highly polarized photoluminescence and photodetection from single indium phosphide nanowires," *Science*, vol. 293, no. 5534, pp. 1455–1457, Aug. 2001.
[34] J. Schneider, W. L. Zhang, A. K. Srivastava, V. G. Chigrinov, H. S. Kwok, and A. L. Rogach, "Photoinduced micropattern alignment of semiconductor nanorods with polarized emission in a liquid crystal polymer matrix," *Nano Lett.*, vol. 17, no. 5, pp. 3133–3138, May 2017.
[35] T. Du *et al.*, "Combination of photoinduced alignment and self-assembly to realize polarized emission from ordered semiconductor nanorods," *ACS Nano*, vol. 9, no. 11, pp. 11049–11055, Nov. 2015.
[36] A. K. Srivastava, W. L. Zhang, J. Schneider, A. L. Rogach, V. G. Chigrinov, and H. S. Kwok, "Photoaligned nanorod enhancement films with polarized emission for liquid-crystal-display applications," *Adv. Mater.*, vol. 29, no. 33, Sep. 2017, Art. no. 1701091.
[37] L. Carbone *et al.*, "Synthesis and micrometer-scale assembly of colloidal CdSe/CdS nanorods prepared by a seeded growth approach," *Nano Lett.*, vol. 7, no. 10, pp. 2942–2950, Oct. 2007.
[38] K. M. Ryan, A. Mastroianni, K. A. Stancil, H. T. Liu, and A. P. Alivisatos, "Electric-field-assisted assembly of perpendicularly oriented nanorod superlattices," *Nano Lett.*, vol. 6, no. 7, pp. 1479–1482, Jul. 12, 2006.
[39] M. Mohammadimasoudi *et al.*, "Fast and versatile deposition of aligned semiconductor nanorods by dip-coating on a substrate with interdigitated electrodes," *Opt. Mater. Exp.*, vol. 3, no. 12, pp. 2045–2054, Dec. 2013.
[40] S. Kaur *et al.*, "Functional film with electric-field-aided aligned assembly of quantum rods for potential application in liquid crystal display," *Adv. Opt. Mater.*, vol. 6, no. 17, 2018, Art. no. 1800235.
[41] B. T. Diroll, N. J. Greybush, C. R. Kagan, and C. B. Murray, "Smectic nanorod superlattices assembled on liquid subphases: Structure, orientation, defects, and optical polarization," *Chem. Mater.*, vol. 27, no. 8, pp. 2998–3008, Apr. 2015.
[42] M. Zanella *et al.*, "Self-assembled multilayers of vertically aligned semiconductor nanorods on device-scale areas," *Adv. Mater.*, vol. 23, no. 19, pp. 2205–2209, May 2011.
[43] F. Pietra *et al.*, "Semiconductor nanorod self-assembly at the liquid/air interface studied by in situ GISAXS and ex situ TEM," *Nano Lett.*, vol. 12, no. 11, pp. 5515–5523, Nov. 2012.
[44] M. Nadasan, T. Visan, D. Moraru, and A. Manea, "Synthesis of colloidal core/shell nanorods and their alignment," *Revista De Chimie*, vol. 62, no. 9, pp. 894–898, Sep. 2011.
[45] A. Persano *et al.*, "Photoconduction properties in aligned assemblies of colloidal CdSe/CdS nanorods," *ACS Nano*, vol. 4, no. 3, pp. 1646–1652, Mar. 2010.
[46] J. Q. Zhuang *et al.*, "Cylindrical superparticles from semiconductor nanorods," *J. Amer. Chem. Soc.*, vol. 131, no. 17, pp. 6084–6085, May 6, 2009.
[47] A. B. Panda, G. Glaspell, and M. S. El-Shall, "Microwave synthesis of highly aligned ultra narrow semiconductor rods and wires," *J. Amer. Chem. Soc.*, vol. 128, no. 9, pp. 2790–2791, Mar. 8, 2006.
[48] T. Wang *et al.*, "Self-assembled colloidal superparticles from nanorods," *Science*, vol. 338, no. 6105, pp. 358–363, Oct. 2012.
[49] S. Ahmed and K. M. Ryan, "Self-assembly of vertically aligned nanorod supercrystals using highly oriented pyrolytic graphite," *Nano Lett.*, vol. 7, no. 8, pp. 2480–2485, Aug. 2007.
[50] S. Yan, L. Lu, H. Meng, N. Huang, and Z. Xiao, "Scalable alignment and transfer of nanowires based on oriented polymer nanofibers," *Nanotechnology*, vol. 21, no. 9, Mar. 5, 2010.
[51] M. Hasegawa, Y. Hirayama, and S. Dertinger, "Polarized fluorescent emission from aligned electrospun nanofiber sheets containing semiconductor nanorods," *Appl. Phys. Lett.*, vol. 106, no. 5, Feb. 2, 2015, Art. no. 051103.
[52] Y. Amit, A. Faust, I. Lieberman, L. Yedidya, and U. Banin, "Semiconductor nanorod layers aligned through mechanical rubbing," *Physica Status Solidi A-Appl. Mater. Sci.*, vol. 209, no. 2, pp. 235–242, Feb. 2012.
[53] P. T. K. Chin, R. A. M. Hikmet, S. C. J. Meskers, and R. A. J. Janssen, "Energy transfer and polarized emission in cadmium selenide nanocrystal solids with mixed dimensionality," *Adv. Functional Mater.*, vol. 17, no. 18, pp. 3829–3835, Dec. 17, 2007.
[54] M. Schierhorn, S. W. Boettcher, S. Kraemer, G. D. Stucky, and M. Moskovits, "Photoelectrochemical performance of CdSe nanorod arrays grown on a transparent conducting substrate," *Nano Lett.*, vol. 9, no. 9, pp. 3262–3267, Sep. 2009.
[55] S. Kang *et al.*, "Capillary printing of highly aligned silver nanowire transparent electrodes for high-performance optoelectronic devices," *Nano Lett.*, vol. 15, pp. 7933–7942, 2015.
[56] M. Gao, L. H. Li, W. B. Li, H. H. Zhou, and Y. L. Song, "Direct writing of patterned, lead-free nanowire aligned flexible piezoelectric device," *Adv. Sci.*, vol. 3, no. 8, Aug. 2016, Art. no. 1600120.
[57] K. F. Wu *et al.*, "Universal length dependence of rod-to-seed exciton localization efficiency in type I and quasi-type II CdSe@CdS nanorods," *ACS Nano*, vol. 9, no. 4, pp. 4591–4599, Apr. 2015.
[58] Y. Huang, X. Duan, Q. Wei, and C. M. Lieber, "Directed assembly of one-dimensional nanostructures into functional networks," *Science*, vol. 291, no. 5504, pp. 630–633, 2001.
[59] S. Vezzoli *et al.*, "Exciton fine structure of CdSe/CdS nanocrystals determined by polarization microscopy at room temperature," *ACS Nano*, vol. 9, pp. 7992–8003, 2015.